A Resonance-Enhanced Multiphoton Ionization and Zero Kinetic Energy Photoelectron Study of the Phenol·Kr and Phenol·Xe van der Waals Complexes

Susanne Ullrich, György Tarczay,† and Klaus Müller-Dethlefs*

Department of Chemistry, The University of York, Heslington, York YO10 5DD, United Kingdom

Received: June 19, 2001; In Final Form: October 4, 2001

Time-of-flight mass spectrometry (TOF-MS), resonance-enhanced multiphoton ionization (REMPI), and zero kinetic energy (ZEKE) photoelectron spectroscopy were employed to study the phenol·Kr and phenol·Xe van der Waals (vdW) complexes in their neutral excited (S_1) and cationic ground (D_0) state. For each complex, excitation and ionization energies and their red shifts relative to the corresponding data for bare phenol were determined. Inter- and intramolecular vibrational frequencies were recorded for the S_1 state of the neutral complex, which were used as intermediate resonances for the observation of vibrational modes of the cationic state. Possibilities of different structures, that is, above ring position of the rare gas atom and "hydrogen-bonded"-like (HB) isomer, were investigated. Finally, the present results are compared to available data on similar systems, for example, phenol·Rg and other complexes of rare gas atoms with aromatic molecules.

Introduction

Weakly bound van der Waals (vdW) complexes have been the subject of a considerable number of spectroscopic investigations. The prototypes of such systems are the benzene·Rg (Rg = Ne, Ar, Kr, and Xe)[1−4] complexes, but several monosubstituted C_6H_5X·Rg (X = F, Cl, CH_3, C≡CH, OH, and NH_2)[5−10] and symmetrical, para-substituted $C_6H_5Y_2$·Ar (Y = F, Cl, CH_3)[9,11,12] series have also been studied. In those studies, excitation, ionization, and interaction energies and intermolecular vibrational frequencies were measured, and red shifts were determined. From these observations, conclusions could be drawn on the effect of polarizability of the rare gas on the strength of the vdW bond and the structure adopted by the dimer.

Benzene·Rg complexes are the simplest systems of this type. The high symmetry of the benzene ring and the isotropic polarizability of the rare gas lead to a highly symmetric cluster structure in which the rare gas atom is located above the center of the benzene ring. Due to the weak interaction, intermolecular vibrations occur in the low-energy region, and they are therefore easily distinguishable from intramolecular modes of benzene. These complexes have three intermolecular vibrational modes: the stretching mode (s_z) is a movement of the rare gas atom perpendicular to the ring along the *z*-axis and the bending modes (b_x and b_y) are displacements above the plane along the *x*-(parallel with one of the C−H bonds) and *y*-axes (perpendicular to the *x*-axis). Intramolecular benzene modes are nearly unaffected by the weakly bound rare gas atom. The structures of benzene·Rg complexes have been determined accurately by high-resolution studies[3,13] to be symmetric top. The equilibrium distance (r_e) of the Rg atom from the center of the benzene ring could be also determined by the extrapolation of the vibrationally averaged rotational constants.

Substitution of one aromatic hydrogen atom with a different functional group leads to a reduction of symmetry of the complex and a possible displacement of the rare gas atom from the center of the ring. As an example, the effect of different substituents on the vibrational structure of the S_1 state of the chlorobenzene·Rg, the phenol·Rg, and the toluene·Rg (Rg = Ne, Ar, Kr, and Xe) complexes due to electronic, inertia, and asymmetry effects has been studied in great detail by Mons et al.[9] The main conclusions of this work and the abovementioned studies are as follows: (a) Similarly to benzene·Rg complexes, the spectral red shift of the $S_1 \leftarrow S_0$ transition, as well as the stretching force constant, correlates with the polarizability of Rg and with the strength of the vdW interaction. (b) Plotting of the stretching force constant of benzene·Ar, *para*-difluorobenzene·Ar and *para*-dichlorobenzene·Ar complexes as a function of red shift defines a straight line; except for aniline·Ar, the unsymmetrically substituted complexes are located far from this line, which was explained by asymmetry effects caused by the X substituent. (c) In contrast to benzene·Rg complexes, because of the reduced symmetry, not only the even bending levels but every bending level is observed. (d) The relative intensity of the bending progressions increases in the series from Ar (or where available from Ne) to Xe, which could be interpreted by the increasing change in geometry during the excitation. (e) Some accidental overlapping (e.g., $2b_x$ and $2b_y$ vibrations in the S_1 state of phenol·Ar), as well as Fermi resonances (e.g., $2b_x$ and s_z, as well as $2b_y$ and s_z, vibrations in the S_1 state of phenol·Kr) has been identified by the careful comparison of the series from Ar (Ne) to Xe.

While Φ·Rg (where Φ is an aromatic molecule) systems have been studied extensively experimentally, ab initio studies are rather sparse. This is due to the fact that high-level ab initio calculations including correlation and basis set superposition error (BSSE) correction are needed to describe weak bonds based on the dispersion interaction(s).[14] So far, detailed computational studies have concentrated on the benzene·Ar system.[14−17] The phenol·Ar system, however, might be of particular interest because the OH group might allow the Rg complex to adopt a "hydrogen-bonded"-like (HB) structure in the symmetry plane. The existence of such a stable HB isomer in the S_0 and D_0 states was predicted by recent ab initio

* To whom correspondence should be addressed. E-mail: kmd6@york.ac.uk. Fax: +44 1904 434527.

† Permanent address: Department of General and Inorganic Chemistry, Eötvös University, P.O. Box 32, H-1518 Budapest 112, Hungary.

10.1021/jp0123379 CCC: $22.00
Published on Web 01/31/2002

calculations.[5,18] In the S_0 state, the counterpoise-corrected MP2/Chal[19] interaction energy (359 cm^{-1}) of the HB isomer is higher than the interaction energy (173 cm^{-1}) of the vdW isomer, whereas in the D_0 state, ROMP2/Chal calculations predict the HB structure being more stable than the vdW isomer.[18,20] (However, these theoretical predictions might change using larger basis sets and theoretical methods taking into account higher-order correlations.) In an experimental reinvestigation[21] of phenol·Ar with particular interest in searching for different isomeric structures, no evidence of a significant formation of the HB isomer under supersonic jet conditions could be found using multiphoton ionization detection. The observation of small spectral red shifts, low intermolecular vibrational modes, and only minor shifts of the phenol OH stretching frequency in the complex[22] and the analysis of the rotational contours[23] unambiguously identified the vdW structure as the only observable isomer in the S_1 and D_0 states. Direct ionization of phenol·Ar complexes by electron impact ionization together with infrared detection, however, lead to the observation of both the vdW and HB isomers.[24]

The aim of this investigation of the phenol·Kr and phenol·Xe complexes was to probe whether the comparatively higher polarizability of the Rg ligand could lead to formation of the HB structure under supersonic jet conditions and its observation by multiphoton ionization. Resonance-enhanced multiphoton ionization (REMPI) and zero kinetic energy (ZEKE) spectra of both complexes are presented in this paper, which show great similarity to the spectra of the vdW-bonded phenol·Ar complex. In addition, the spectra presented allow a comparison with the series of phenol·Rg complexes in their S_1 and D_0 states and comparison of systems within these series, as well as to series of related Φ·Rg complexes.

Experimental Section

The experimental setup and techniques employed have been described in detail before[25,26] and will therefore only be summarized briefly here. The complexes were produced in a supersonic jet expansion of phenol seeded in a Rg/Ar or Rg/Ne mixture (ratio 1:7). Phenol (Fluka >99.5%, without any further purification) was heated to 100 °C in a sample holder located directly behind the nozzle (General Valve series 9, orifice 600 μm). The skimmed molecular beam interacts with the counterpropagating excitation and ionization lasers. The produced ions/electrons are extracted employing pulsed fields onto the perpendicularly arranged ion and electron optics. Electrons and ions are detected on multichannel plates, the ions being focused by a reflectron. The pulse sequences, timings, and field strengths used to ionize the Rydberg states are identical to those described in refs 25 and 27.

The excimer (Lambda-Physik EMG 1003i) pumped two-color laser system consisted of Radiant Narrowscan (Coumarin 153) and Lambda-Physik FL3002 (Sulforhodamine B) dye lasers, which were both KDP frequency doubled. Simultaneously recorded iodine[28] spectra were used to calibrate the REMPI spectra, while phenol and phenol·argon were used as internal standards to obtain field-free, calibrated ionization energies. The accuracy of wavelength calibrations are assumed to be 1 and 5 cm^{-1}, respectively, for the S_1 and D_0 states.

Results and Discussion

Time-of-Flight (TOF) Spectra. The REMPI time-of-flight spectra of phenol·Kr and phenol·Xe are shown in Figure 1. Both rare gas complexes show several mass peaks in the TOF spectrum corresponding to the different rare gas isotopes.

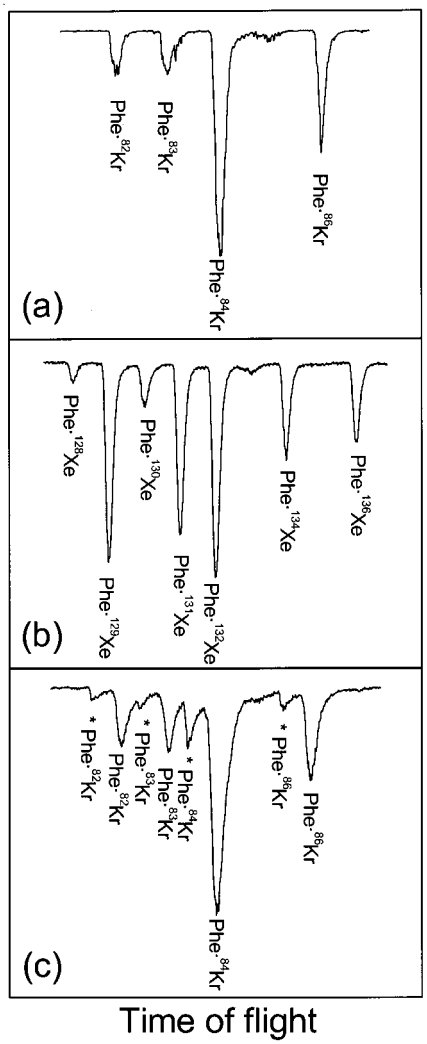

Figure 1. REMPI time-of-flight spectra of (a) phenol·Kr and (b) phenol·Xe recorded with the excitation laser set to the corresponding $S_1 \leftarrow S_0$ resonance. The MATI time-of-flight spectrum of phenol·Kr is presented in panel c.

Krypton has six stable isotopes with masses of 77.9, 79.9, 81.9, 82.9, 83.9, and 85.9 u and with corresponding natural occurrences of 0.35%, 2.25%, 11.6%, 11.5%, 57.0%, and 17.3%, respectively. The latter four isotopomers were observed as different mass peaks in the complex TOF spectrum, while the first two isotopes were below the detection limit. The natural occurrences of the isotopes are represented by the signal intensity of the corresponding mass peaks (Figure 1a).

Similarly, for xenon, which has six dominant isotopes with masses of 128.9, 129.9, 130.9, 131.9, 133.9, and 135.9 u and with corresponding natural occurrences of 26.4%, 4.1%, 21.2%, 26.9%, 10.4%, and 8.9%, its complex shows the time-of-flight spectrum displayed in Figure 1b. The other isotopomers below 2% occurrence are not detected.

The time-of-flight spectrum of phenol·Kr recorded under conditions set up for the mass-analyzed threshold ionization (MATI) experiment is shown in Figure 1c. The MATI signal, observed for each isotopomer when the ionization laser is tuned to the ionization energy, appears at a slightly earlier TOF separated from the spontaneous ions signals. This demonstrates the difficulty in separating spontaneous and MATI ions and demonstrates why high-resolution MATI[37] was unavailable in this study.

REMPI. The REMPI spectra presented here were recorded with a time gate set on the most abundant isotopomer. Within

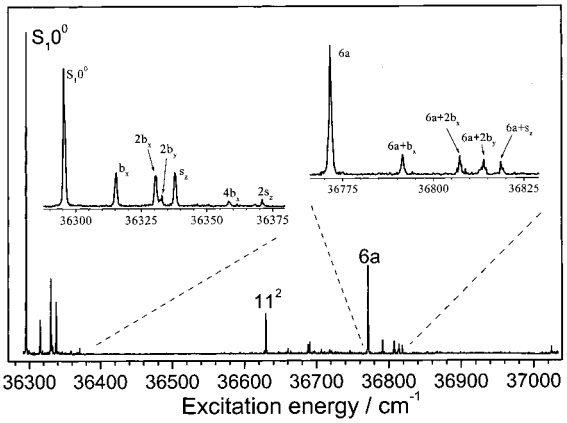

Figure 2. Long-range two-color REMPI spectrum of phenol·Kr with the ionization laser set to 32 121 cm^{-1}.

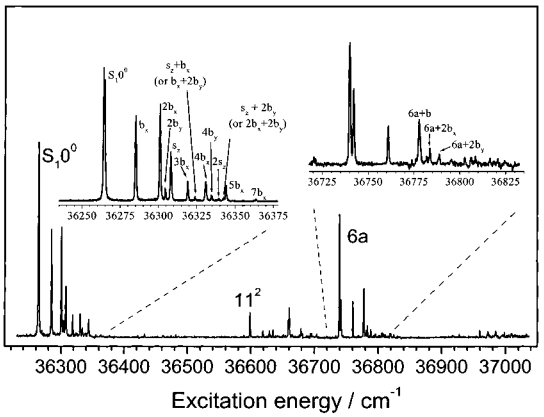

Figure 3. Long-range two-color REMPI spectrum of phenol·Xe with the ionization laser set to 32 147 cm^{-1}.

TABLE 1: Frequencies and Assignments of the Vibrational Bands Observed in the REMPI Spectrum of Phenol·Krypton

assignment		excitation energy, cm^{-1}	internal energy, cm^{-1}	intensity
intramolecular mode	intermolecular mode			
0^0	0^0	36 295.6	0	s
	b_x	36 315.8	20.2	m
	$2b_x$	36 330.8	35.2	m
	$2b_y$	36 333.2	37.6	vw
	s_z	36 338.4	42.8	m
	$4b_x$	36 359.1	63.5	vw
	$2s_z$	36 371.2	75.6	vw
11^2	0^0	36 629.6	334.0	m
	b_x	36 647.6	352.0	vw
	s_z	36 660.4	364.8	vw
	$2b_x$	36 663.9	368.3	vw
	$4b_x$	36 688.4	392.8	w
	$2s_z$	36 690.6	395.0	w
	$5b_x$	36 706.9	411.3	vw
	$3s_z$ (or $6b_x$)	36 718.4	422.8	vw
6a	0^0	36 771.5	475.9	s
	b_x	36 791.5	495.9	m
	$2b_x$	36 807.3	511.7	m
	$2b_y$	36 813.9	518.3	m
6b	0^0	36 818.6	523.0	m

the experimental resolution, frequency shifts between the different isotopomers could not be observed, and the REMPI spectra for all time gates were identical. For both complexes, all features observed in the two-color REMPI spectra (Figures 2 and 3) in the regions up to 700 cm^{-1} above the origin transitions and their assignments are summarized in Tables 1 and 2.

TABLE 2: Frequencies and Assignments of the Vibrational Bands Observed in the REMPI Spectrum of Phenol×e1·Xenon

assignment		excitation energy, cm^{-1}	internal energy, cm^{-1}	intensity
intramolecular mode	intermolecular mode			
0^0	0^0	36 264.0	0.0	s
	b_x	36 284.8	20.8	s
	$2b_x$	36 300.7	36.7	s
	$2b_y$	36 304.4	40.4	w
	s_z	36 307.8	43.8	m
	$3b_x$	36 318.5	54.5	w
	s_z+b_x (or b_x+2b_y)	36 324.1	60.1	vw
	$4b_x$	36 330.4	66.4	w
	$4b_y$	36 334.0	70.0	vw
	$2s_z$	36 338.3	74.3	vw
	s_z+2b_x (or $2b_x+2b_y$)	36 341.6	77.6	vw
	$5b_x$	36 343.7	79.7	w
	$7b_x$	36 362.9	98.9	vw
11^2	0^0	36 598.5	334.5	w
	b_x	36 618.7	354.7	vw
	s_z	36 629.1	365.1	vw
	$2b_x$	36 635.0	371.0	vw
	$2s_z$	36 660.5	396.5	w
	$5b_x$	36 679.0	415.0	vw
	$3s_z$ (or $6b_x$)	36 693.9	429.9	vvw
	$7b_x$	36 703.9	439.9	vvw
6a	0^0	36 739.2	475.2	s
	resonance?	36 741.7	477.7	m
	b_x	36 760.3	496.3	m
	$2b_x$	36 777.4	513.4	m
	$2b_y$	36 781.6	517.6	vw
	s_z	36 783.1	519.1	vw
6b	0^0	36 788.2	524.2	vw

REMPI Spectrum of Phenol·Kr. The REMPI spectrum of phenol·Kr is displayed in Figure 2 with the inserts showing an expansion of the S_1 origin and the 6a intramolecular region with intermolecular vibrations built upon them. This long-range two-color REMPI spectrum with the probe laser set to 32 121 cm^{-1} replicates the previously recorded one-color REMPI spectrum by Mons et al.[9] very well with much better quality and extends the spectral information into the intramolecular region. The most intense feature appears at 36 295.6 ± 1 cm^{-1}, which can be assigned to the $S_1 \leftarrow S_0$ origin transition. This corresponds to a red shift of 56.5 ± 1 cm^{-1} from the S_1 origin of bare phenol (36 348.7 ± 1 cm^{-1}),[29] which is in good agreement with the values of Mons et al.[9] (55 cm^{-1}) and Ebata et al.[22] (56 cm^{-1}).

The low-frequency region of the REMPI spectrum displays the three intermolecular vibrations and their overtones. The features at 20.2 ± 1 cm^{-1}, 35.2 ± 1 cm^{-1}, 37.6 ± 1 cm^{-1}, and 42.8 ± 1 cm^{-1} can be assigned by comparison to other phenol·Rg complexes[9] to b_x, $2b_x$, the first overtone of the other bend ($2b_y$), and the intermolecular stretch s_z, respectively, followed by higher overtones, $4b_x$ and $2s_z$.

In the investigated higher-energy region above 36 600 cm^{-1}, four intramolecular modes are observed, which can be assigned by comparison to the phenol monomer REMPI spectrum. The two strong features at 334.0 ± 1 cm^{-1} and 475.9 ± 1 cm^{-1} are the 11^2 and 6a Wilson[30] modes. Whereas the 6a in-plane ring mode is unaffected by the Rg atom, the out-of-plane ring mode 11^2 shows a frequency blue shift of 9.6 cm^{-1} compared to the monomer transition at 324.4 cm^{-1}, a common observation in aromatic·Rg complexes. While the less intense peak at 523.0 cm^{-1} can be assigned to the 6b, the one at 729.0 cm^{-1} remains ambiguous. One possibility would be the 12 mode, which appeared in bare phenol at 783.1 cm^{-1}.[31]

The overall modest intramolecular vibrational structure of the REMPI spectrum can be attributed to only small geometry

changes upon S_1 excitation. Notable however, is the occurrence of combination bands of intermolecular vibrations built upon the 6a mode. The features at 495.9 ± 1 cm^{-1}, 511.7 ± 1 cm^{-1}, and 518.3 ± 1 cm^{-1} relative to the S_1 origin band can be assigned to 6a + b_x, 6a + $2b_x$ and 6a + s_z, respectively. Similar but less intense intermolecular modes can be observed on the 11^2: 352.0 cm^{-1} ($11^2 + b_x$), 364.8 cm^{-1} ($11^2 + s_z$), 368.3 cm^{-1} ($11^2 + 2b_x$), 392.8 cm^{-1} ($11^2 + 4b_x$), 395.0 cm^{-1} ($11^2 + 2s_z$), 411.3 cm^{-1} ($11^2 + 5b_x$), and 422.8 cm^{-1} ($11^2 + 3s_z$). It is interesting to note that the intermolecular stretch occurs at a much lower frequency (around 30 cm^{-1}) when excited in combination with the 11^2 than without intramolecular excitation. This can be explained by the fact that 11^2 is a symmetric out-of-plane CH mode.

REMPI Spectrum of Phenol·Xe. Overall, the phenol·Xe complex displays vibrational structure in the REMPI spectrum very similar to phenol·Kr. The long-range two-color REMPI spectrum displayed in Figure 3 was recorded with the ionization laser set to 32 147 cm^{-1} and shows good agreement in the low-frequency region to the previously recorded one-color spectrum recorded by Mons et al.[9] The dominant feature at 36 264.0 ± 1 cm^{-1} can be assigned to the vibrationless $S_1 \leftarrow S_0$ origin transition and corresponds to a red shift of 88.1 ± 1 cm^{-1} from bare phenol.

In the low-frequency region just above the $S_1 \leftarrow S_0$ transition, several intermolecular vibrations including their overtones and combination modes are observed. The b_x and its overtones $2b_x$, $3b_x$, $4b_x$, $5b_x$, and possibly $7b_x$ are located at 20.8 ± 1, 36.7 ± 1, 54.5 ± 1, 66.4 ± 1, 79.7 ± 1, and 98.9 ± 1 cm^{-1} above the origin band. Further bend overtones $2b_y$ and $4b_y$ occur at 40.4 ± 1 and 70.0 ± 1 cm^{-1}, and the stretching vibration s_z and its overtone $2s_z$ occur at 43.8 ± 1 and 74.3 ± 1 cm^{-1}. Additionally, with relatively weak intensity, the combination mode $s_z + b_x$ and its overtone $s_z + 2b_x$ are observed at 60.1 ± 1 and 77.6 ± 1 cm^{-1}, respectively. Features with more than four quanta of excitation in b_x, the overtone of the intermolecular stretch $2s_z$, and the combination band $b_x + b_y$ and its overtone could be identified in this study because of a better signal-to-noise ratio compared to the previously published one-color REMPI spectrum.[9]

The observation of more extensive vibrational excitation in the intermolecular region compared to the phenol·Kr complex is possibly due to a slightly larger geometry change in the phenol·Xe complex occurring upon excitation. Another difference between the phenol·Kr and phenol·Xe complexes is the change of the intensity ratio of the origin peak and the peaks corresponding to bending modes. While the S_1 origin transition is the most dominant feature in the spectrum of phenol·Kr, in the case of the phenol·Xe complex the low-frequency intermolecular modes gain intensity because of larger Franck−Condon (FC) factors.

In the higher-frequency region, the intramolecular Wilson[30] modes 11^2, 6a, and 6b can be assigned as 334.6 ± 1, 475.2 ± 1, and 524.2 cm^{-1}, respectively. The intermolecular vibrations building upon the 6a ring mode can be assigned to 6a + b_x (496.3 ± 1 cm^{-1}), 6a + $2b_x$ (513.6 ± 1 cm^{-1}), 6a + $2b_y$ (517.5 ± 1 cm^{-1}), and 6a + s_z (519.1 ± 1 cm^{-1}). A long but very weak progression of intermolecular modes occurs in combination with the 11^2: 354.7 cm^{-1} ($11^2 + b_x$), 365.1 cm^{-1} ($11^2 + s_z$), 371.0 cm^{-1} ($11^2 + 2b_x$), 396.5 cm^{-1} ($11^2 + 2s_z$), 415.0 cm^{-1} ($11^2 + 4b_x$), 429.9 cm^{-1} ($11^2 + 3s_z$) and 439.9 cm^{-1} ($11^2 + 5b_x$). It is also interesting to note that the 6a vibrational mode is split in the S_1 state. This is probably due to an accidental overlap with other vibrational mode.

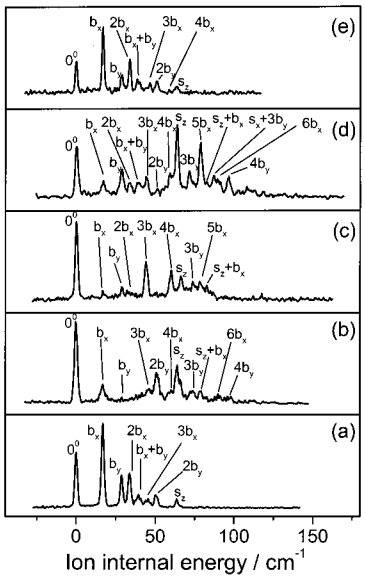

Figure 4. ZEKE spectra of phenol·Kr recorded via different intermediate vibrational states of the S_1 excited state: (a) via S_1 origin; (b) via b_x; (c) via $2b_x$; (d) via s_z; (e) via 6a.

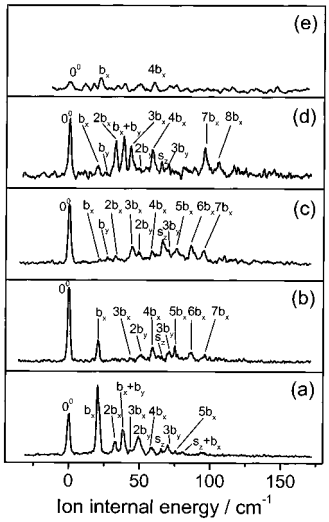

Figure 5. ZEKE spectra of phenol·Xe recorded via different intermediate vibrational states of the S_1 excited state: (a) via S_1 origin; (b) via b_x; (c) via $2b_x$; (d) via s_z; (e) via 6a.

ZEKE. The ZEKE spectra of phenol·Kr and phenol·Xe recorded via (a) the S_1 origin and, additionally, to help the assignment, via several vibrationally excited modes, (b) the bending mode S_1 b_x (c) its overtone S_1 $2b_x$, (d) the intermolecular stretch S_1 s_z and (e) the intramolecular ring mode S_1 6a, are displayed in Figures 4 and 5 relative to their ion internal energy. The spectral features observed in the ZEKE spectra of both complexes, as well as their assignments, are listed in Tables 3 and 4. Because no frequency shifts were observed for the same $S_1 \leftarrow S_0$ transitions of the different isotopomers, all of them contribute to the ZEKE spectra.

ZEKE Spectra of Phenol·Kr. The ZEKE spectrum of phenol·Kr recorded via the S_1 0^0 band origin is shown in Figure 4a. The lowest energy feature at 68 394 cm^{-1} can be identified as the ionization energy, which is red-shifted relative to the ionization energy of phenol by 234 cm^{-1}. Built upon this band are distinct progressions of the bending modes (b_x and b_y). This pattern is similar to the one observed in the ZEKE spectrum of the phenol·Ar complex.[21] The movement of the Rg along the *x*-axis (i.e., along the C−O bond of phenol)[32] upon the ionization

TABLE 3: Assignments of the Observed Bands in the ZEKE Spectra of Phenol·Krypton Recorded via Different S_1 Intermediate States

	ion internal energy, cm^{-1}				
assignment	via 0^0	via b_x	via $2b_x$	via s_z	via 6a
0^0	0 s	0 s	0 s	0 s	0 s
b_x	17 s	17 m	16 vw	17 m	17 s
b_y	29 m	29 vw	29 vw	29 m	29 m
$2b_x$	34 m	31 vw	32 vw	34 w	34 s
$b_x + b_y$	39 w	38 vw	38 vw	39 w	38 m
$3b_x$	45 w	46 vw	44 m	45 w	46 w
$2b_y$	50 w	51 w	51 vw	51 w	51 w
$4b_x$		60 m	60 w	59 w	59 vw
s_z	64 w	64 m	66 w	64 s	63 w
$3b_y$		74 w	74 vw	72 m	
$5b_x$		78 w	78 vw	79 s	
$s_z + b_x$		83 vw	83 vw	83 vw	
$3b_y + b_x$		88 vw		87 w	
$6b_x$		90 vw		90 w	
$4b_y$		98 vw		97 w	

TABLE 4: Assignments of the Observed Bands in the ZEKE Spectra of Phenol·Xenon Recorded via Different S_1 Intermediate States

	ion internal energy, cm^{-1}				
assignment	via 0^0	via b_x	via $2b_x$	via s_z	via 6a
0^0	0 s	0 s	0 s	0 s	0 s
b_x	20 s	21 m	22 vw	20 vw	21 s
b_y		26 vw	27 vw	26 vw	
$2b_x$	33 m	33 vw	33 vw	33 m	
$b_x + b_y$	38 m	37 vw	36 vw	38 m	
$3b_x$	44 vw	43 vw	45 vw	43 m	
$2b_y$	49 m	51 w	49 w	49 vw	
$4b_x$	59 w	59 w	58 m	58 m	59 s
s_z	65 w	66 w	66 m	65 w	
$3b_y$	70 m	71 w	70 w	70 w	
$5b_x$	76 vw	75 m	76 m	73 vw	
$s_z + b_x$	78 vw	79 vw	80 vw	81 w	
$6b_x$		86 w	86 m		
$7b_x$		96 w	95 m	96 m	
$8b_x$			106 vw	106 w	

leads to the observation of a distinct progression of b_x with a frequency of 16.9 cm^{-1}. This value is close to the one observed for phenol·Ar (15 cm^{-1})[21] and related complexes such as chlorobenzene·Ar (15 cm^{-1}) and fluorobenzene·Ar (13 cm^{-1}).[33,34] The occurrence of a progression of this mode up to three quanta ($2b_x$ at 33.8 cm^{-1} and $3b_x$ at 45.5 cm^{-1} ion internal energy) suggests that a geometry change occurs along this axis upon ionization. Despite an increase in binding energy upon ionization, a decrease in frequency of the b_x mode is observed, which must result from a flatter potential energy surface for this mode in the cationic complex. This observation was also made in previous studies on other Ar vdW complexes. The frequencies of the other bending mode b_y (by 10 cm^{-1}) and the stretching mode s_z (by 21 cm^{-1}) show an increase in frequency upon ionization confirming the stronger interaction.

The feature of medium intensity at 28.6 cm^{-1} ion internal energy can tentatively be assigned to the other bending mode b_y, with the overtone $2b_y$ occurring at 50.3 cm^{-1} and a combination band of the two bends $b_x + b_y$ at 40.3 cm^{-1}. The intermolecular stretch s_z is observed at 63.7 cm^{-1}.

The ZEKE spectrum recorded via the S_1 b_x intermediate resonance is displayed in Figure 4b. The bending mode b_x is observed at 16.8 cm^{-1} followed by a long progression of overtones up to six quanta, while the other bending mode b_y shows a progression of up to four quanta. The intermolecular stretch occurs at 63.8 cm^{-1} with medium intensity. Some combination bands between the two bends and with the stretch are possibly observed. The ZEKE spectrum recorded via the first overtone of the S_1 b_x bending mode has similar structure but with the noteable difference that the b_x fundamental is hardly observable.

Similarly long progressions (up to six quanta of the b_x, four quanta of the b_y) and the same combination bands as in the ZEKE spectrum via the intermediate b_x mode are observed for the spectrum recorded via the S_1 s_z mode (Figure 4d). Frequencies and their assignments are listed in the Table 3. The intermolecular stretch at 63.9 cm^{-1} becomes the most intense feature of the spectrum. The ZEKE spectrum recorded via the intramolecular S_1 6a mode (Figure 4e) overall resembles the one recorded via the S_1 0^0 origin but shows a few additional features of higher overtones.

The main purpose of recording ZEKE spectra through different intermediate vibrations of the S_1 state is to observe changes in intensity of the different vibrational modes in the ZEKE spectrum that originate from geometry changes and therefore FC overlaps between the S_1 and D_0 states. Comparison of the overall appearance of the ZEKE spectra shows that ionization via intermediates without intermolecular excitation (i.e., via S_1 0^0 and 6a) results in a ZEKE spectrum in which the intermolecular bend b_x dominates over all other peaks including the ionization energy. This suggests that a geometry change occurs upon ionization in which the Kr atom shifts along the *x*-axis. Because the interaction energy due to charge-induced polarization is larger in the D_0 state than in the S_1 state and the positive charge is partially delocalized onto the O-atom, the equilibrium position of the rare gas is expected to move toward the phenol group OH.

A shift of the FC envelope toward higher ion internal energies is observed in ZEKE spectra recorded via intermediates with intermolecular vibrational excitation. If the $\Delta v = 0$ propensity rule[35] were strictly followed, an enhancement of the mode corresponding to the intermediate excitation should be observed in the ZEKE spectrum. Independent of which mode was excited in the S_1 state progressions of the bending modes, b_x and b_y are observed, and additionally, combination bands with the stretch with both having the maximum intensity shifted toward higher frequencies are observed. The b_x mode is no longer the dominant peak of the ZEKE spectra; in fact, it becomes nearly unobservable in the spectrum recorded via the $2b_x$. In the ZEKE spectrum recorded via the S_1 s_z mode, the stretching mode in the cation becomes the most intense feature.

ZEKE Spectra of Phenol·Xe. Observations in the ZEKE spectra of phenol·Xe are overall more or less analogous to those in the phenol·Kr complex and will only be briefly summarized. The discussion will therefore concentrate on differences between the two complexes.

The ZEKE spectrum of phenol·Xe recorded via the S_1 0^0 band origin is presented in Figure 5a. The ionization energy of phenol·Xe and its red shift relative to phenol are determined to be 68 302 and 326 cm^{-1}, respectively. As in the ZEKE spectra of phenol·Ar and phenol·Kr, distinct progressions of the bending modes b_x and b_y occur. The fundamental of the b_x mode is observed at 20.4 cm^{-1} followed by overtones up to five quanta. Whereas the fundamental of the bending mode b_y could not be identified, the second and third quanta of excitation of this mode appeared at 49.2 and 70.2 cm^{-1}, and a combination mode $b_x + b_y$ occurred at 38.2 cm^{-1}. The intermolecular stretch occurs at 65.4 cm^{-1} and in combination with the b_x mode at 78.3 cm^{-1}.

A significant difference of phenol·Xe compared to phenol·Kr lies in the b_x mode. As mentioned before, the observation in several Φ·Ar and the phenol·Kr complexes was that, despite

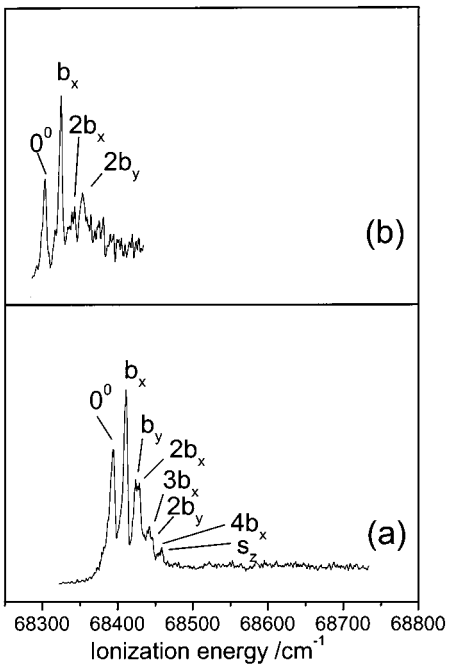

Figure 6. MATI spectra of (a) phenol·Kr and (b) phenol·Xe recorded via the respective S_1 origins.

an increase in binding energy upon ionization, the frequency of the b_x mode decreased. In the phenol·Xe complex, however, the bending mode b_x occurs at identical frequencies in the S_1 and D_0 spectra. This indicates that intermolecular potential for this mode is very similar in shape in both states.

The ZEKE spectrum recorded via the S_1 b_x intermediate resonance is displayed in Figure 5b. The bending mode b_x (21.0 cm^{-1}) shows up to seven quanta. In contrast to the ZEKE spectrum recorded via the S_1 origin, the fundamental of the b_y (26.5 cm^{-1}) is observed when intermolecular vibrational excitation was already present in the S_1 state. The FC envelope however is shifted to higher overtones of the bending modes. The intermolecular stretch occurs at 65.6 cm^{-1}. As in the ZEKE spectra via the S_1 origin, combination bands between the b_x and the b_y and s_z modes are observed.

The ZEKE spectrum recorded via the first overtone of the S_1 b_x bending mode shows a very similar structure, but as in phenol·Kr, the intensity of the b_x fundamental is considerably reduced. Additionally, the b_x mode progression can be identified up to seven or probably eight quanta of excitation at 95 and 106 cm^{-1}.

Figure 5d displays the ZEKE spectrum recorded via the S_1 s_z mode. The frequencies of possibly up to nine quanta of the b_x and three quanta of the b_y mode are listed in Table 4 including combination bands. In contrast to the phenol·Kr complex, the ionization energy peak is the most intense feature.

The ZEKE spectrum recorded via the intramolecular S_1 6a (Figure 5e) shows some vibrational features, but only those of strong intensity at 0, 21, and 59 cm^{-1} could be unambiguously identified as 0^0, b_x, and $4b_x$. Finally, it should also be noted, that in the ZEKE spectra recorded via vibrationally excited S_1 states the peak corresponding to the D_0 0^0 state becomes the dominant feature.

MATI. To exclude the possible contribution to the ion spectra of bigger clusters due to accidental coincidences of bands in the S_1 state, the MATI spectra of the phenol·Kr (Figure 6a) and phenol·Xe (Figure 6b) complexes have been also recorded via the S_1 0^0 origin band of the most abundant isotopomer. MATI ionization energies were calibrated to the corresponding ZEKE origin. All of the main intensive features observed in the ZEKE spectra are identified in the MATI spectra, too. Both the frequencies and the intensities are in very good agreement with the ZEKE spectra. As a consequence of the smaller resolution and the lower signal-to-noise ratio,[36] some vibrations are not clearly resolved and the weak intensity modes observed in the ZEKE spectra were below the detection limit. Although the resolution attainable by ZEKE spectroscopy, and consequently the investigation of spectral shifts due to "isotopic substitution" of the Rg atom, could be achieved using the high-resolution MATI technique,[37] the close appearance of the different isotopomers in the TOF spectra and the low intensity of the isotopomers peaks made this method unavailable in our case.

Conclusions

In this study, we have presented the REMPI, ZEKE, and MATI spectra of phenol·Kr and phenol·Xe. These complexes, as well as the previously studied phenol·Ar complex, have similar spectra. The most pronounced features are the b_x progressions in almost all cases. This observation indicates the dislocation of Rg along the C−O bond axes of phenol both upon excitation and upon ionization. On the other hand, the similar frequency values corresponding to the S_1 and D_0 states indicate that the shapes of the bending potentials of these two states are similar.

The red shifts corresponding to the $S_1 \leftarrow S_0$ and $D_0 \leftarrow S_0$ transitions of the investigated complexes, together with literature values of similar Φ·Rg complexes, are collected in Table 5. The observed red shift of the 0^0 $S_1 \leftarrow S_0$ band origin is 56.5 cm^{-1} for phenol·Kr and 88.1 cm^{-1} for phenol·Xe. For the 11^2 $S_1 \leftarrow S_0$ transition, 10 and 11 cm^{-1} blue shifts are observed for the two complexes. The red shifts of the adiabatic ionization energies are much larger than the red shifts of the 0^0 $S_1 \leftarrow S_0$ band origins, 234 and 326 cm^{-1}, respectively. The ratio of the red shifts of the $D_0 \leftarrow S_0$ and the $S_1 \leftarrow S_0$ band origins decreases with the polarizability of Rg. The ratio is 5.3 for phenol·Ar, 4.3 for phenol·Kr, and 3.8 for phenol·Xe, which can be compared with the corresponding ratios of fluorobenzene·Ar (9.5), chlorobenzene·Ar (7.0), aniline·Ar (2.0), and aniline·Kr (1.4).

As a comparison, REMPI and ZEKE spectra of phenol and phenol·Rg (from Ar to Xe) are shown in Figure 7. Because of the increase of the polarizability of the Rg atom, the most conspicuous difference among the REMPI spectra of the complexes is the increasing FC factors of the overtones from Ar to Xe. As an example, in the spectrum of phenol·Ar, only b_x and its first overtone, $2b_x$, could be identified, and in the case of phenol·Kr, additionally $4b_x$ could be identified, while in the REMPI spectrum of phenol·Xe, even $5b_x$ and $7b_x$ could be identified. A similar tendency can be seen for the intramolecular modes, as well as for the combination of inter- and intramolecular modes. The increase of the FC factors of the higher overtones is much less significant in the case of ZEKE spectra, which also reveal that the polarizability of Rg is less important in the D_0 than in the S_1 state.

The intermolecular vibrational frequencies in the S_1 state are almost identical for the three complexes. This is due to the compensation of two effects, the increase of the intermolecular interaction and the increase of the mass of the Rg atom. The only notable difference among the three spectra is the increasing separation of the two bending modes (and possibly the increasing coupling among the three intermolecular modes). In the case of ZEKE spectra, the change of the b_x bending mode is much

TABLE 5: Observed Red Shifts of the $S_1 \leftarrow S_0$ and $D_0 \leftarrow S_0$ Transitions of Some Φ·Rg

	$S_1 \leftarrow S_0$					$D_0 \leftarrow S_0$		
		red shift					red shift	
molecule/complex	EE[a]	0^0	6a	11^2	6b	IE[b]	0^0	ref(s)
benzene	38 606[c]					74 211		38, 39
benzene·Ar	38 585[c]	−21[c]				74 383	−172	38, 39
benzene·Kr	38 572[c]	−33[c]				74 322	−233	38, 39
benzene·Xe	38 552	−54[c]						39
phenol	36 349					68 628		31
phenol·Ar	36 316	−33	+4	+15		68 452	−176	21
phenol·Kr	36 294	−56	0	+10		68 394	−234	this work, 9, 22
phenol·Xe	36 262	−88	0	+11	+1	68 302	−326	this work, 9
chlorobenzene	37 048					73 173		9
chlorobenzene·Ar	37 021	−27				72 984	−189	9, 33
chlorobenzene·Kr	37 007	−41						9
chlorobenzene·Xe	36 984	−64						9
fluorobenzene	37 818					74 238		7
fluorobenzene·Ar	37 794	−24				74 011	−227	7
aniline	34 035					62 266		8
aniline·Ar	33 982	−54				62 153	−113	8
aniline·Kr	33 951	−84				62 121	−144	8

[a] Absolute value of the $S_1 \leftarrow S_0$ excitation energy. [b] Absolute value of the $D_0 \leftarrow S_0$ ionization energy. [c] Excitation energies and red shifts of the 6^1_0 band. The vibrationless $S_1 \leftarrow S_0$ transition is symmetry-forbidden.

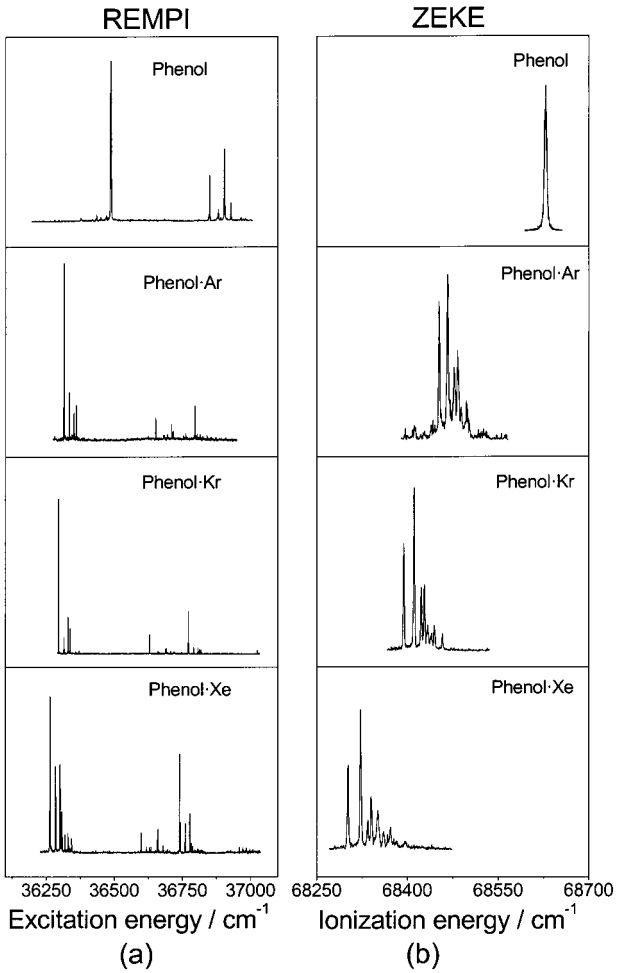

Figure 7. (a) REMPI and (b) ZEKE spectra of phenol and phenol·Rg.

more pronounced; it increases from 15 to 20 cm^{-1} from Ar to Kr, but the change is not significant for the b_y and s_z modes. Finally, because the overall appearance of the REMPI and ZEKE spectra of phenol·Kr and phenol·Xe closely resembles that of the vdW-bonded phenol·Ar spectra and all features within their spectra could be assigned (except the band next to the 6a mode in the REMPI spectrum of phenol·Xe), it can be concluded that, independent of the rare gas, under supersonic conditions the HB isomer cannot be observed using multiphoton ionization detection.

Acknowledgment. We thank the EPSRC for financial support (Chemistry GR/L27770). The authors thank Dr. Caroline E. H. Dessent and Mr. M. S. Ford for helpful discussions. S.U. acknowledges support from the Fonds des Verbandes der Chemischen Industrie followed by a DAAD Doktorandenstipendium im Rahmen des gemeinsamen Hochschulsonderprogramms III von Bund und Ländern. The work of G.T. has been partially supported by the Hungarian Scientific Research Fund (OTKA T032489); his stay at The University of York was supported by an Eötvös Scholarship of the Hungarian Ministry of Education and by the Peregrinatio II Foundation. He also thanks Profs. L. Szepes and A. G. Császár for their generous help.

References and Notes

(1) Müller-Dethlefs, K.; Dopfer, O.; Wright, T. G. *Chem. Rev.* **1994**, *94*, 1845.

(2) Müller-Dethlefs, K.; Hobza, P. *Chem. Rev.* **2000**, *100*, 143.

(3) Neusser, H. J.; Krause, H. *Chem. Rev.* **1994**, *94*, 1829.

(4) Garret, A. W.; Pribble, R. N.; Gotch, A. J.; Zwier, T. S. Resonant Two-Photon Ionization Studies of C_6H_6-X_n Clusters. In *Advances in Multiphoton Processes and Spectroscopy*; Villaeyes, A. A., Fujimura, Y., Eds.; World Scientific: Singapore, 1994; Vol. 9.

(5) Dessent, C. E. H.; Müller-Dethlefs, K. *Chem. Rev.* **2000**, *100*, 3999.

(6) Bieske, E. J.; Rainbird, M. W.; Atkinson, I. M.; Knight, A. E. W. *J. Chem. Phys.* **1989**, *91*, 752.

(7) Shinohara, H.; Sato, S.; Kimura, K. *J. Phys. Chem. A* **1997**, *101*, 6736.

(8) Jäckel, J.-G.; Jones, H. *Chem. Phys.* **1999**, *247*, 321.

(9) Mons, M.; Le Calvé, J.; Piuzzi, F.; Dimicoli, I. *J. Chem. Phys.* **1990**, *92*, 2155.

(10) Dao, P. D.; Morgan, S.; Castleman, A. W. *Chem. Phys. Lett.* **1984**, *111*, 38.

(11) Jacobson, B. A.; Humphrey, S.; Rice, S. A. *J. Chem. Phys.* **1988**, *89*, 5624.

(12) Dao, P. D.; Morgan, S.; Castleman, A. W. *Chem. Phys. Lett.* **1985**, *113*, 219.

(13) Weber, Th.; von Bargen, A.; Riedle, E.; Neusser, H. J. *J. Chem. Phys.* **1990**, *92*, 90.

(14) Koch, H.; Fernández, B.; Christiansen, O. *J. Chem. Phys.* **1998**, *108*, 2784.

(15) Hobza, P.; Bludský, O.; Selze, H. L.; Schlag, E. W. *Chem. Phys. Lett.* **1996**, *250*, 402.

(16) Koch, H.; Fernández, B.; Makarewicz, J. *J. Chem. Phys.* **1999**, *111*, 198.

(17) Hobza, P.; Bludský, O.; Selze, H. J.; Schlag, E. W. *J. Chem. Phys.* **1992**, *97*, 335.

(18) Chapman, D. M. Ph.D. Thesis, The University of York, York, U.K., 1998.

(19) The Chal basis set is the combination of two basis sets: the 6-31G* basis set for the elements C, H, and O and for Ar the 7s4p2d1f basis set as described in: Chałsiński, G.; Kendall, R. A.; Simons, J. *J. Chem. Phys.* **1987**, *89*, 3569. Chałsiński, G.; Cybulski, S. M.; Szczęsníak M. M.; Scheiner, S. *J. Chem. Phys.* **1989**, *91*, 7809.

(20) The counterpoise-corrected interaction energy is determined to be 669 cm^{-1} for the HB isomer and 538 cm^{-1} for the vdW isomer.

(21) Haines, S. R.; Dessent, C. E. H.; Müller-Dethlefs, K. *J. Electron Spectrosc.* **2000**, *108*, 1.

(22) Fujii, A.; Sawamura, T.; Tanabe, S.; Ebata, T.; Mikami, N. *Chem. Phys. Lett.* **1994**, *225*, 104.

(23) Ford, M. S.; Haines, S. R.; Pugliesi, I.; Dessent, C. E. H.; Müller-Dethlefs, K. *J. Electron Spectrosc.* **2000**, *112*, 231.

(24) Solcà, N.; Dopfer, O. *Chem. Phys. Lett.* **2000**, *325*, 354.

(25) Haines, S. R.; Geppert, W. D.; Chapman, D. M.; Watkins, M. J.; Dessent, C. E. H.; Cockett, M. C. R.; Müller-Dethlefs, K. *J. Chem. Phys.* **1998**, *109*, 9244.

(26) Ullrich, S.; Geppert, W. D.; Dessent, C. E. H.; Müller-Dethlefs, K. *J. Phys. Chem. A* **2000**, *104*, 11864.

(27) Dietrich, H.-J.; Müller-Dethlefs, K.; Baranov, L. Y. *Phys. Rev. Lett.* **1996**, *76*, 3530.

(28) Gerstenkorn, S.; Luc, P. *Atlas du Spectra d'Absorption de la Molécule d'Iode*; CNRS: Paris, 1980.

(29) Martinez, S. J., III; Alfano, J. C.; Levy, D. H. *J. Mol. Spectrosc.* **1992**, *152*, 80.

(30) Wilson, E. B. *Phys. Rev.* **1934**, *45*, 706.

(31) Dopfer, O. Zero Kinetic Energy (ZEKE) Photoelektronenspektroskopie an wasserstoffbrückengebundenen Phenolkomplexen. Dissertation, Technische Universität München, 1994.

(32) Zhang, X.; Knee, J. L. *Faraday Discuss.* **1994**, *97*, 299.

(33) Lembach, G.; Brutschy, B. *Chem. Phys. Lett.* **1997**, *273*, 421.

(34) Lembach, G.; Brutschy, B. *J. Chem. Phys.* **1997**, *107*, 6156.

(35) Müller-Dethlefs, K.; Schlag, E. W. *Angew. Chem., Int. Ed.* **1998**, *37*, 1346.

(36) In contrast to the ZEKE method in which all isotopes contribute to the spectra, the mass selective detection of MATI leads to a lower signal-to-noise ratio.

(37) Dessent, C. E. H.; Haines, S. R.; Müller-Dethlefs, K. *Chem. Phys. Lett.* **1999**, *315*, 103.

(38) Krause, H.; Neusser, H. J. *J. Chem. Phys.* **1993**, *99*, 6278.

(39) Weber, Th.; Riedle, E.; Neusser, H. J.; Schlag, E. W. *Chem. Phys. Lett.* **1991**, *183*, 77.